Effect of heat treatment on corrosion behaviour of welded AA6061 aluminium alloy in seawater

Nur Azhani Abd Razak[1], **A Juliawati**[1], **LH Shah**[1], and **M Ishak**[1,2]
[1]Faculty of Mechanical Engineering, Universiti Malaysia Pahang, 26600 Pekan, Pahang, Malaysia
[2]Automotive Engineering Centre, Universiti Malaysia Pahang, 26600 Pekan, Pahang, Malaysia

E-mail: azhani@ump.edu.my, juliawati@ump.edu.my, luqmanhakim@ump.edu.my, and mahadzir@ump.edu.my

Abstract. The effect of various heat treatments on the corrosion behaviour of welded AA6061 aluminium alloy was investigated. Gas tungsten arc welding (GTAW) was used for welding butt joint specimens. Corrosion behaviour was determined in seawater solution using potentiodynamic polarization method. Microstructure and compositional analysis of base metal (BM) and weld metal (WM) was studied with scanning electron microscope (SEM) and energy dispersive spectroscopy (EDS). The result indicated that BM consists of Fe-rich coarse intermetallic particles that behave as cathodic sites with respect to the matrix. Tafel plot showed that WM is cathode and give better corrosion resistance in different heat treatment compared to BM. Localized corrosion was observed on the corroded surfaces by SEM.

1. Introduction

Magnesium and silicon are two major alloying elements in the 6xxx series of wrought aluminium alloys. These series of aluminium alloys are widely used for lightweight structures in automotive and aerospace industries due to their good extrudability, weldability, and excellent corrosion resistance [1-4]. Other than that, these type of alloys are also age hardenable, and usually heat treated to both T4 (solution heat treatment and naturally aging) and T6 (solution heat treatment and artificially aging) temper conditions in order to develop adequate strength [3-6]. In Al-Mg-Si alloys, a great increase in strength is caused by the precipitates formed from solution of merely 1 wt% of Mg and Si that is added to Al [7]. However, in the commercial aluminium alloys, impurity elements such as Fe and Mn are always present. Even not large amount of these impurities causes the formation of a new phase component. The exact composition of the alloy and the casting condition will directly influence the selection and volume fraction of intermetallic phases. During casting of 6xxx aluminium alloys a wide variety of Fe-containing intermetallics phases are formed between the aluminium dendrites [8]. A few previous studies have found that iron-containing intermetallic particles could influence the corrosion behaviour of aluminium alloys [9-10]. The particles that exist in the microstructure could significantly reduce the resistance to localized corrosion [10]. The corrosion behaviour of these intermetallic particles depends mainly upon their potential difference with respect to the matrix in the solution. Particles which are electrochemically more noble than the matrix act as cathodes whereby the surrounding matrix undergoes anodic dissolution. This process could lead to localized corrosion [10].

[1] Faculty of Mechanical Engineering, Universiti Malaysia Pahang, 26600 Pekan, Pahang, Malaysia

Welding as a fabrication method is an important manufacturing technology in the aluminium alloy industry [11-12]. The development of the inert gas shielded welding processes of metal inert gas (MIG) and tungsten inert gas (TIG) have made it possible for joining aluminium alloys. However, several problems may exist when attention is focused on heat-treatable alloys such as 6xxx series as heat generated by the welding process could lead to deterioration in mechanical properties due to phase transformation and softening induced in the alloys [13]. Differences in composition and microstructure of fusion zone (FZ) or heat affected zone (HAZ) relative to the base metal (BM) can create an electrochemical potential difference between the zones and cause galvanic corrosion. [11, 14].

The aim of this present study is to investigate the combined effects of heat treatment and welding process on the corrosion behaviour of AA6061 aluminium alloy which utilizes ER4047 filler wire.

2. Experimental procedure

2.1. Materials

Materials used in this study were 2 mm thin sheet of AA6061 aluminium alloy in annealed condition and 1.6 mm diameter of ER4047 filler metal. Chemical compositions of the materials used are given in Table 1. The chemical composition was obtained by using optical emission spectrometer (Model: Foundry Master).

Table 1. Chemical composition (wt.%) of AA6061 aluminium alloy and ER4047 filler metal.

Alloy	Mg	Si	Fe	Cr	Cu	Mn	Al
AA6061	0.89	0.53	0.20	0.20	0.30	0.02	Balance
ER4047	0.10	11.00	0.80	-	0.30	0.15	Balance

2.2. Welding process

GTAW was employed to join the plates together. The butt welding process was performed with ER4047 filler metal. All the necessary care was taken to avoid joint distortion and the joints were made after securing the plates with suitable clamps. Prior to welding, the base materials were cleaned by using ultrasonic cleaning. The selective GTAW process parameters are shown in Table 2.

Table 2. Parameters of GTAW process.

Base current	40 A
Frequency	2 Hz
Pulse on time	40 %
Background current	20 A

2.3. Heat treatment process

The plates of this alloy were subjected to a series of heat treatment, which is given in Table 3.

Table 3. Heat treatment process of AA6061 aluminium alloy

Sample ID	Condition
1	As-received, welded without any heat treatment
2	As-received, T6 tempered and then welded
3	As-received, welded and then T6 tempered
4	As-received, solution heat treated, water quenched, aged at room temperature for 7 hours and finally welded

In all samples, solution heat treatment was carried out at 530 °C for 45 minutes in a furnace. The artificial aging was performed at 175 °C in a furnace for 8 hours [5, 8, 11].

2.4. Structural characterization and hardness measurement

Surface preparations of the samples were prepared by standard metallographic techniques which consists of wet grinding with various grit abrasive papers, mechanical polishing by using the diamond compound (0.05μm particle size), and then etching by immersing in Keller solution (2.5% HNO_3, 1.5% HCl, 1.0% HF, and 95% distilled water). Scanning electron microscopy (SEM) and energy dispersive spectroscopy (EDS) techniques (Model: JEOL JSM-7600F) were used to study the microstructure and morphology of the samples after welding process.

2.5. Electrochemical testing

WonATech model WPG100 potentiostat and IVMan 1.2 software were used for monitoring the corrosion potentials of the base metal and weld metal as well as potentiodynamic polarization measurements. The photograph of the potentiodynamic polarization setup is shown in Figure 1. The experimental setup for the electrochemical measurements consisted of a three-electrode cell with the sample as a working electrode of exposed area 14 mm^2, a saturated calomel electrode (SCE) as a reference electrode and a graphite rod as the counter electrode. The working electrode was placed in the cell with the seawater solution. Measurements for the polarization curves were recorded in the potential range of -1000 to 1000 mV and at the scan rate of 4 mV s^{-1}. The anodic and cathodic polarization curves were obtained for each specimen and corrosion potentials and corrosion current densities were determined by Tafel extrapolation and linear polarization methods.

(a) (b)

Figure 1. Potentiodynamic polarization setup : (a) Electrochemical measurement setup and (b) WPG100 potentiostat.

3. Results and discussion

3.1. Microstructural characteristics

Microstructures of weld metal (WM), partially melted zone (PMZ), heat affected zone (HAZ) and base metal (BM) of AA6061 aluminium alloy in as-welded condition (Sample 1) are shown in Figure 2.

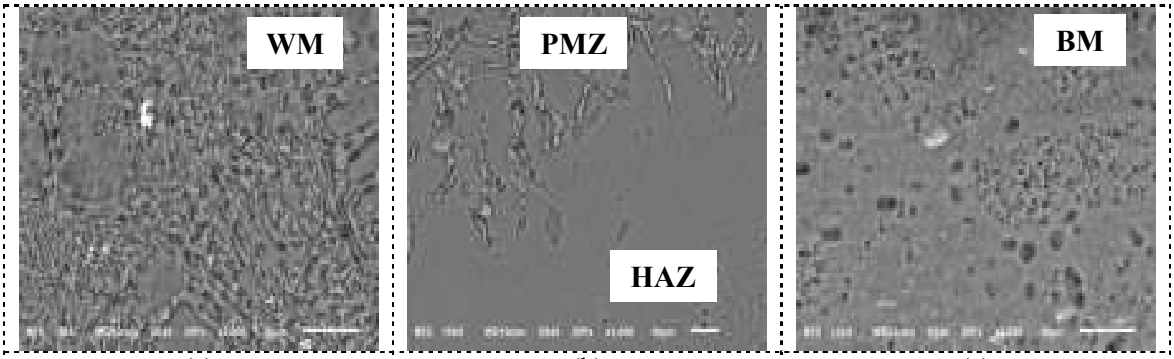

Figure 2. SEM images of AA6061 aluminium alloy in as-welded condition (Sample 1): (a) WM (2000x magnification), (b) PMZ and HAZ (1000x magnification) and (c) BM (2000x magnification).

SEM images of the BM of samples in different conditions are also shown in Figure 3. Based on the figure, irregular distribution of coarse particles throughout the BM is clearly observed in all conditions. This is in line with the study conducted by Nikseresht [11]. The coarse particles are believed to be formed during casting [8].

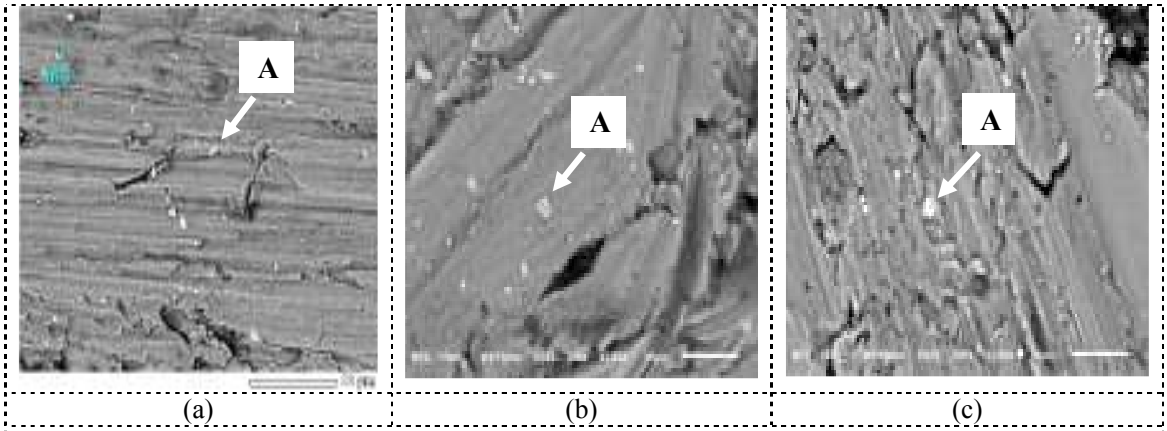

Figure 3. Backscattered images of BM of AA6061 aluminium alloy: (a) Sample 1, (b) Sample 2 and (c) Sample 4.

EDS analysis revealed that Al, Fe, Si, Cr and Mg elements are present in these coarse particles which can be seen in Table 4. Some researchers have also found the intermetallic compounds in their studies [11, 15-16]. Based on Table 4, Fe is the main impurity element that forms these particles. It can be attributing to the very slow solubility of Fe in the aluminium matrix [11].

Table 4. EDS analysis (wt.%) of coarse particles in AA6061 aluminium alloy (A area in Fig. 2).

	Al	Fe	Si	Cr	Mn	Mg
Sample 1						
A	62.94	24.01	3.78	2.98	1.65	4.64
Sample 2						
A	66.62	27.16	1.94	1.20	1.62	1.46
Sample 4						
A	74.77	19.80	1.68	1.08	1.84	0.83

Table 4 also revealed the decreased of magnesium content of these particles in Sample 2 and Sample 4 due to heat treatment process. That phenomenon is caused by the high diffusion coefficient of Mg in aluminium matrix [11]. In addition, it is noticed that the heat treatment processes have changed the morphology of the coarse particles from irregular shape (Figure 2a) to almost globular (Figure 2b and c).

Figure 4 shows the weld metal microstructures for Sample 1 and Sample 3. According to the figure, eutectic structure and precipitated intermetallic particles are present in the interdendritic spaces of α-Al matrix. These two constituents can be differentiated by grey and light regions respectively.

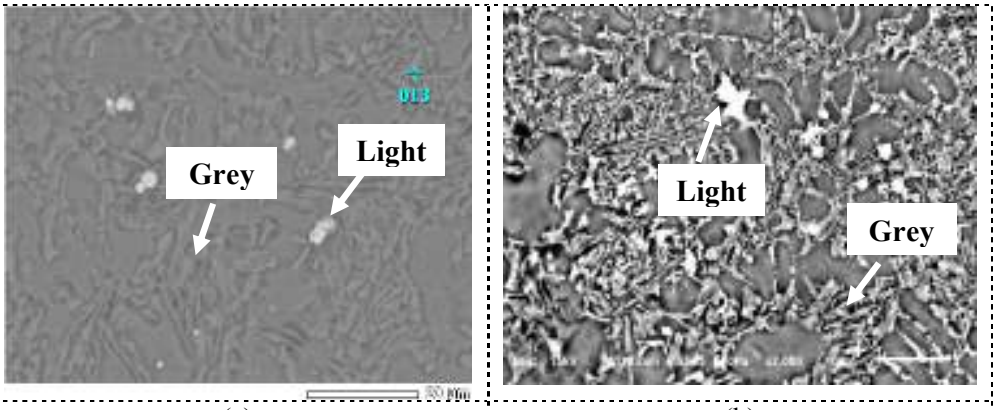

Figure 4. SEM images of WM of AA6061 aluminium alloy using ER4047 filler metal (grey and light regions) : (a) Sample 1 and (b) Sample 3.

As can be seen in Table 5, it is obvious that grey eutectic structures in both samples consist of significant amount of Al and Si. Eutectic structure is believed to be enriched by Si element as ER4047 filler metal consists of 11.00 wt.% silicon. On the other hand, the intermetallic compounds which are indicated by light regions consist of Al-Fe-Si and having a small fraction of Mg. High iron concentration in these particles could be due to the composition of filler metal. Significant amount of Mg detected in these intermetallic compounds is contributed by the dilution of the BM towards WM [11].

Table 5. EDS analysis (wt.%) of welded AA6061 aluminium alloy (grey and light regions in Fig. 4).

	Al	Fe	Si	Mg
Sample 1				
Grey regions	86.64	-	13.36	-
Light regions	64.52	25.45	9.84	0.19
Sample 3				
Grey regions	84.87	-	14.49	0.64
Light regions	63.51	26.85	8.41	1.23

3.2. Corrosion behaviour

The BM and WM potentiodynamic polarization curves for sample 1 and sample 2 in seawater solution are shown in Figure 5. The corrosion current densities were determined using Tafel extrapolation method. According to the graph, the WM specimen exhibits a higher corrosion potential in both conditions as compared to the BM specimen. It is attributed to the high silicon content in the

weldment. As mentioned by Nikseresht [11], silicon in solid solution condition has a tendency to increase the dissolution potential of aluminium. Thus, in a galvanic coupling of BM and WM zones, the WM area behaves as cathode and the BM is an anode. Based on results obtained from polarization measurements in Table 6, it is confirmed that heat treatment process would increase the corrosion potential of the BM specimens towards more positive values.

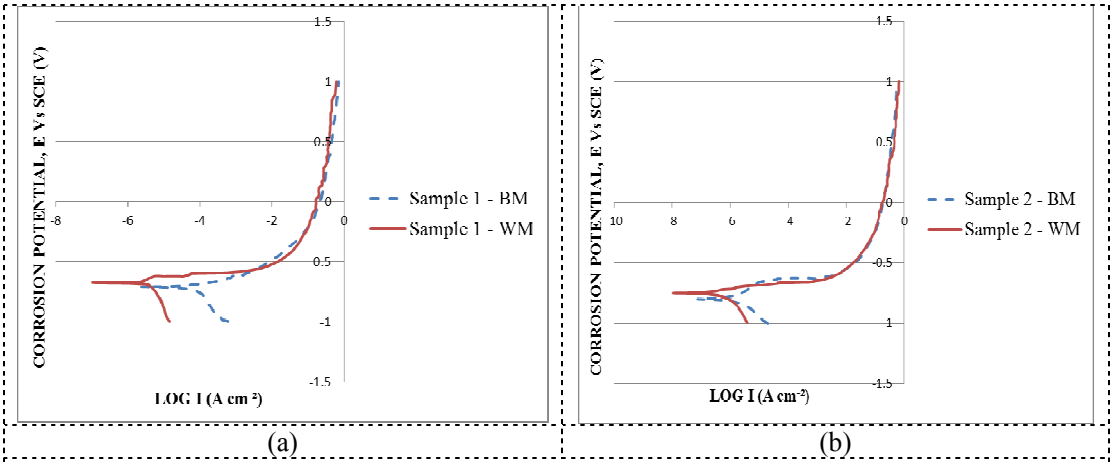

Figure 5. Potentiodynamic polarization curves for base metal and weld metal of AA6061 aluminium alloy weldment using ER4047 filler metal in seawater solution : (a) Sample 1 and (b) Sample 2.

Table 6. Corrosion current density and corrosion potential of AA6061 aluminium alloy weldment in seawater solution.

Sample	E_{corr} (mV)		I_{corr} (nA cm^{-2})	
	BM	WM	BM	WM
1	-734.024	-708.319	2456.604	832.179
2	-715.314	-700.307	2420.465	798.443
3	-710.937	-692.076	2495.726	1138.571
4	-718.677	-697.318	2503.831	968.059

Corrosion potential depends on the electrochemical behaviour of the microstructure and this is directly depends on the quantity of the present phases. Course intermetallic particles that are enriched from iron and silicon would lead to dilution of matrix from these alloying elements [11]. Therefore, dilution of matrix from iron and silicon tends to be the main reason for anodic behaviour of the non-heat-treated BM specimen (Sample 1). According to Nikseresht [11], fine precipitates of magnesium silicide (Mg_2Si) would form and dispersed throughout the matrix during the artificial aging process. These fine precipitates are slightly more anodic than the aluminium matrix. Thus, corrosion potential of the remainder matrix would increase due to dilution of matrix from these elements. Based on Table 6, it is confirmed that there is an increase of corrosion potential in the heat-treated BM specimens.

Table 6 also shows that the tendency for galvanic corrosion (E_{corr} WM - E_{corr} BM) is the highest for Sample 1. The BM showed higher corrosion rate than the WM in all conditions. The higher corrosion rate in BM is contributed by the presence of secondary phases in the microstructure. As mentioned by Nikseresht [11], these coarse particles are enriched with iron. As the composition of these particles is different than the matrix, thus, a potential difference happens between them. Fe-rich intermetallic particles are found to be favourable sites for cathodic reaction as compared to Al matrix.

More cathodic activities are caused by higher number of cathodic particles. This would be the reason of an increase of corrosion rate in BM rather than WM.

The WM has a dendritic structure as shown previously in Figure 4. Eutectic structure and intermetallic phases are present in the interdendritic spaces. These phases normally increase susceptibility to microgalvanic corrosion. Eutectic structures consist of aluminium and silicon whereby intermetallic particles that are present along the eutectic structures are iron rich phases. As mentioned previously, iron rich particles act as cathodic areas with respect to aluminium matrix. The presence of these cathodic areas within the weld zone could affect the corrosion rate of the WM. As a result, higher corrosion rate in BM regions as compared to WM areas could be from the effect of higher iron content in the coarse particles and its irregular distribution pattern as illustrated in Figure 3.

Figure 6 shows that all specimens suffer from localized corrosion when they are observed by SEM after the potentiodynamic polarization measurements. Morphology of the surface confirmed that the coarse particles behave as nucleation sites for pitting. Some other regions showed the initiation of matrix dissolution while the iron rich particles were unaffected. This can be seen from Figure 6(b).
Dendritic structure of the WM is susceptible to localized corrosion. Preferential corrosion occurred adjacent to eutectic silicon and iron rich intermetallic phases as observed in all specimens. SEM observation shows that localized corrosion occur at the WM as illustrated in Figure 7.

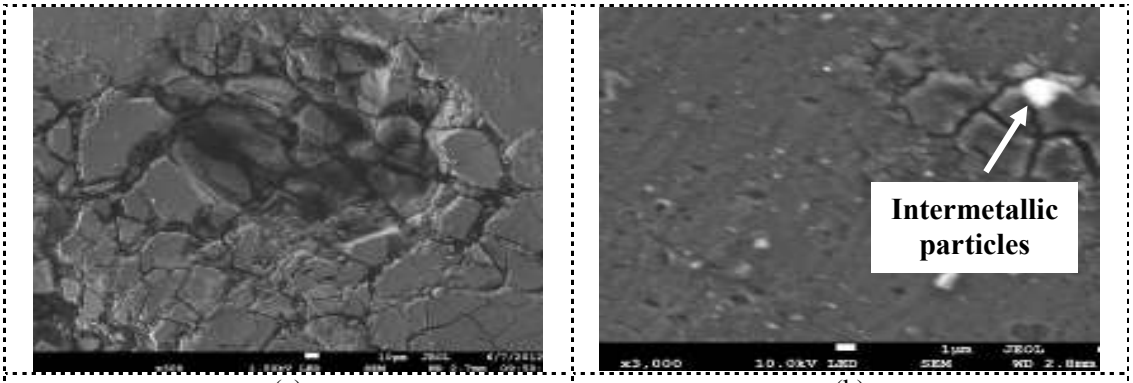

Figure 6. Morphology of the surface after potentiodynamic polarization measurements in BM of Sample 1: (a) Localized corrosion (300x magnification) and (b) Initiation of matrix dissolution (3000x magnification).

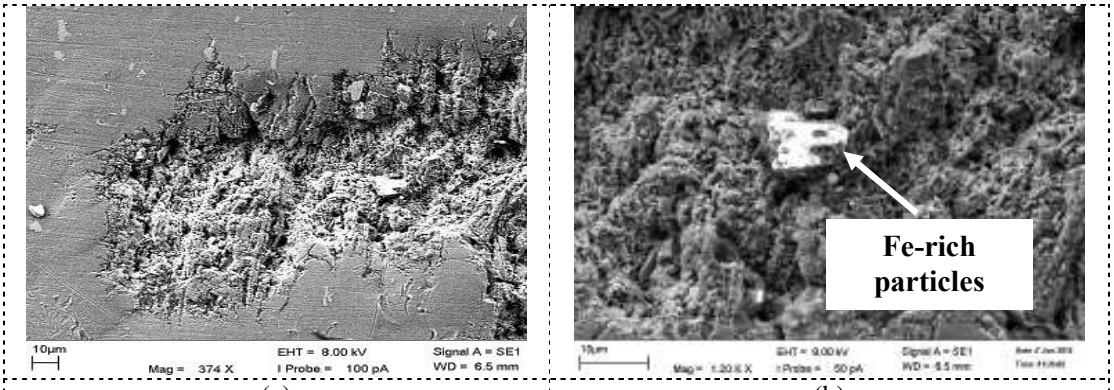

Figure 7. Morphology of the surface after potentiodynamic polarization measurements in WM of Sample 1: (a) Localized corrosion (374x magnification) and (b) Initiation of matrix dissolution around Fe-rich particles (1200x magnification).

4. Conclusion

In this study, the effect of heat treatment on the corrosion behaviour of welded AA6061 aluminium alloy was investigated, and the following conclusions are obtained:

- The WM region behaves as cathode and shows better corrosion resistance under various conditions as compared to the BM area.
- Heat treatment process increases the corrosion potential of the BM specimens towards more positive values.
- Fe-rich coarse metallic particle acts as cathodic sites with respect to the matrix.
- Secondary phases increase the susceptibility of both the BM and WM specimens to localized corrosion.

References

[1] K. El-Menshawy, A. A. El-Sayed, M. A. El-Bedawy, H. A. Ahmed and S. M. El-Raghy: 'Effect of aging time at low aging temperatures on the corrosion of aluminum alloy 6061', *Corrosion Science,* 2012, **54**, 167-173.

[2] H. Agarwal, A. M. Gokhale, S. Graham and M. F. Horstemeyer: 'Void growth in 6061-aluminum alloy under triaxial stress state', *Materials Science and Engineering A,* 2003, **341**, 35-42.

[3] T. Oppenheim, S. Tewfic, T. Scheck, V. Klee, S. Lomeli, W. Dahir, P. Youngren, N. Aizpuru, R. Clark, E. W. Lee, J. Ogren and O. S. Es-Said: 'On the correlation of mechanical and physical properties of 6061-T6 and 7249-T76 aluminum alloys', *Engineering Failure Analysis,* 2007, **14**, 218-225.

[4] D. Maisonnette, M. Suery, D. Nelias, P. Chaudet and T. Epicier: 'Effects of heat treatments on the microstructure and mechanical properties of a 6061 aluminium alloy', *Materials Science and Engineering A,* 2011, **528** 2718-2724.

[5] G. A. Edwards, K. Stiller, G. L. Dunlop and M. J. Couper: 'The precipitation sequence in Al-Mg-Si alloys', *Acta Mater.,* 1998, **46**, 3893-3904.

[6] M. K. Abbass, H. A. Ameen and K. S. Hassan: 'Effect of heat treatment on corrosion resistance of friction stir welded AA2024 aluminum alloy', *American Journal of Scientific and Research,* 2011, **2**, 297-306.

[7] S. J. Andersen, H. W. Zandbergen, J. Jansen, C. Traeholt, U. Tundal and O. Reiso: 'The crystal structure of the β″ pahse in Al-Mg-Si alloys', *Acta Mater*., 1998, **46**, 3283-3298.

[8] G. Mrowka-Nowotnik and J. Sieniawski: 'Influence of heat treatment on the microstructure and mechanical properties of 6005 and 6082 aluminum alloys', *Journal of Materials Processing Technology*, 2005, **162-163**, 367-372.

[9] R. Ambat, A. J. Davenport, G. M. Scamans and A. Afseth: 'Effect of iron-containing intermetallic particles on the corrosion behaviour of aluminium', *Corrosion Science*, 2006, **48**, 3455-3471.

[10] Z. Szklarska-Smialowska: 'Pitting corrosion of aluminium', *Corrosion Science*, 1999, **41**, 1743-1767.

[11] Z. Nikseresht, F. Karimzadeh, M. A. Golozar and M. Heidarbeigy: 'Effect of heat treatment on microstructure and corrosion behaviour of Al6061 alloy weldment', *Materials and Design*, 2010, **31**, 2643-2648.

[12] A. B. M. Mujibur Rahman, S. Kumar and A. R. Gerson: 'Galvanic corrosion of laser weldments of AA6061 aluminum alloy', *Corrosion Science,* 2007, **49,** 4339-4351.

[13] A. Squillace, A. D. Fenzo, G. Giorleo and F. Bellucci: 'A comparison between FSW and TIG welding techniques: modifications of microstructure and pitting corrosion resistance in AA2024-T3 butt joints', *Journal of Materials Processing and Technology*, 2004, **152**, 97-105.

[14] F. Karimzadeh, M. Heidarbeigy and A. Saatchi: 'Effect of heat treatment on corrosion behaviour of Ti-6Al-4V alloy weldments', *Journal of Materials Processing and Technology*, 2008, **206**, 388-394.
[15] Z. Hu, S. Yuan, X. Wang, G. Liu and Y. Huang: 'Effect of post-weld heat treatment on the microstructure and plastic deformation behaviour of friction stir welded 2024', *Materials and Design*, 2011, **32**, 5055-5060.
[16] M. Jariyaboon, A. J. Davenport, R. Ambat, B. J. Connolly, S. W. Williams and D. A. Price: 'The effect of welding parameters on the corrosion behaviour of friction stir welded AA2024-T351', *Corrosion Science*, 2007, **49**, 877-909.